NASA/TM-20210010199

Electrolytic Co-deposition Neutron Production Evaluation

Phillip J. Smith, Robert C. Hendricks, and Bruce M. Steinetz
Glenn Research Center, Cleveland, Ohio

July 2021

NASA STI Program . . . in Profile

Since its founding, NASA has been dedicated to the advancement of aeronautics and space science. The NASA Scientific and Technical Information (STI) Program plays a key part in helping NASA maintain this important role.

The NASA STI Program operates under the auspices of the Agency Chief Information Officer. It collects, organizes, provides for archiving, and disseminates NASA's STI. The NASA STI Program provides access to the NASA Technical Report Server—Registered (NTRS Reg) and NASA Technical Report Server—Public (NTRS) thus providing one of the largest collections of aeronautical and space science STI in the world. Results are published in both non-NASA channels and by NASA in the NASA STI Report Series, which includes the following report types:

- TECHNICAL PUBLICATION. Reports of completed research or a major significant phase of research that present the results of NASA programs and include extensive data or theoretical analysis. Includes compilations of significant scientific and technical data and information deemed to be of continuing reference value. NASA counter-part of peer-reviewed formal professional papers, but has less stringent limitations on manuscript length and extent of graphic presentations.

- TECHNICAL MEMORANDUM. Scientific and technical findings that are preliminary or of specialized interest, e.g., "quick-release" reports, working papers, and bibliographies that contain minimal annotation. Does not contain extensive analysis.

- CONTRACTOR REPORT. Scientific and technical findings by NASA-sponsored contractors and grantees.

- CONFERENCE PUBLICATION. Collected papers from scientific and technical conferences, symposia, seminars, or other meetings sponsored or co-sponsored by NASA.

- SPECIAL PUBLICATION. Scientific, technical, or historical information from NASA programs, projects, and missions, often concerned with subjects having substantial public interest.

- TECHNICAL TRANSLATION. English-language translations of foreign scientific and technical material pertinent to NASA's mission.

For more information about the NASA STI program, see the following:

- Access the NASA STI program home page at http://www.sti.nasa.gov

- E-mail your question to help@sti.nasa.gov

- Fax your question to the NASA STI Information Desk at 757-864-6500

- Telephone the NASA STI Information Desk at 757-864-9658

- Write to:
  NASA STI Program
  Mail Stop 148
  NASA Langley Research Center
  Hampton, VA 23681-2199

NASA/TM-20210010199

Electrolytic Co-deposition Neutron Production Evaluation

Phillip J. Smith, Robert C. Hendricks, and Bruce M. Steinetz
Glenn Research Center, Cleveland, Ohio

National Aeronautics and
Space Administration

Glenn Research Center
Cleveland, Ohio 44135

July 2021

Acknowledgments

The authors gratefully acknowledge the assistance of many people that supported this effort. For co-deposition protocol and methodology consultation: Mr. Lawrence Forsley and Dr. Pamela Mosier-Boss; technical support during testing: Mr. Kevin Prokopius; and statistical support and consultation: Dr. Christopher Daniels. We are also grateful for Dr. Vadim Lvovich (NASA Glenn) for valuable comments on the manuscript; Ms. Laura Becker's patient editorial attention, and Ms. Lorie Passe's careful manuscript preparation. Funding for this work was provided by NASA Headquarters Planetary Sciences Division, Science Mission Directorate.

Level of Review: This material has been technically reviewed by technical management.

Available from

NASA STI Program
Mail Stop 148
NASA Langley Research Center
Hampton, VA 23681-2199

National Technical Information Service
5285 Port Royal Road
Springfield, VA 22161
703-605-6000

This report is available in electronic form at http://www.sti.nasa.gov/ and http://ntrs.nasa.gov/

Electrolytic Co-deposition Neutron Production Evaluation

Phillip J. Smith, Robert C. Hendricks,* and Bruce M. Steinetz
National Aeronautics and Space Administration
Glenn Research Center
Cleveland, Ohio 44135

Summary

Co-deposition electrochemical cells are a simple means to examine novel nuclear reactions. In this study, palladium and deuterium atoms were co-deposited on a cathode at stoichiometric densities. Bubble detector neutron dosimeters were used to measure equivalent dose levels during electrolytic deposition. Standard configuration cells expected to produce excess neutrons were denoted as experimental cells and contained an electrolyte consisting of palladium(II) chloride, lithium chloride, and heavy water (D_2O). The control cells used copper(II) chloride, lithium chloride, and D_2O electrolyte. Experimental and control cells were supplied current, increasing from 0.1 to 100.0 mA over a period of 20 days. For test days 9 through 20, the standard configuration experimental cells exhibited significantly higher average neutron radiation than the controls at a 99% confidence level. Alternative configurations involving increasing current over a shortened time scale, substitutions of water in place of D_2O or potassium chloride for lithium chloride, as well as inclusion of depleted uranium near the cell cathodes all resulted in inconclusive evidence for promoting neutron production.

Nomenclature

AD	Anderson-Darling
b	number of bubbles in bubble detector
C	control
CR-39	Columbia Resin 39
D	deuterium, deuteride
D_20	heavy water
DI	de-ionized
DU	depleted uranium
E	experimental
H	equivalent dose
HPGe	high-purity germanium gamma detector
p	p-value
S	manufacturer quoted calibrated detector sensitivity in bubbles per microsievert
SA	Sigma-Aldrich
T	trial

*Currently retired.

1.0 Introduction

The purpose of these experiments is to evaluate bubble detectors as real-time dosimeters monitoring the co-deposition process, compare cumulative radiation doses detected near cells with two distinct electrolytic compositions, determine if there are neutron emissions above background levels, show that cells of this chemistry are safe to operate, and review factors that may affect neutron generation. This report is intended to supplement a previously published Journal of Electroanalytical Chemistry article (Ref. 1), which focused on statistical and theoretical analysis of the bubble detector data for a particular experimental configuration that was repeated over seven trials. Statistically significant neutron production was measured near the cells containing palladium compared to the control cells. In addition, other trials were completed that variously incorporated magnets at the cell exterior and depleted uranium in the cell interior, substituted water for heavy water or KCl for LiCl, and utilized Columbia Resin 39 (CR-39) chips for neutron particle observation. Although there is insufficient information to make definitive conclusions for these alternative setups, there is potentially useful information herein to direct future research activity.

2.0 Test Material, Equipment, and Procedures

Test materials were de-ionized (DI) water, Cambridge Isotope Laboratories heavy water (D_2O), International Bio-Analytical Industries depleted uranium (DU), Sigma-Aldrich (SA) palladium(II) chloride ($PdCl_2$), SA copper(II) chloride ($CuCl_2$), SA lithium chloride (LiCl), SA nitric acid (HNO_3), SA potassium chloride (KCl), SA 0.25-mm-diameter gold wire, and SA 0.25-mm-diameter platinum wire.

2.1 Electrolysis Cell Assembly

A test system diagram is shown in Figure 1, including electrical circuits and details of the electrolysis cell interior. The electrodes were placed on opposite sides of the cell, and each were secured on a plastic mesh lattice. A spacer was cut from a polyethylene sheet (approximately 1.3 cm wide and 2.5 cm long) to keep the electrodes upright and prevent contact between them. The platinum and gold wires, each greater than 99.9 percent purity on a trace metals basis, were cut to lengths of ~22 cm for the platinum anode and ~13 cm for the gold cathode. For cleaning, the electrode wires were immersed in a ~2 M nitric acid solution for several minutes then rinsed by placing them in a beaker with DI water. All plastic components and two glass capillary tubes were thoroughly rinsed with DI water. These materials were left to dry completely in air.

In this report, cells that include $PdCl_2$ in the electrolyte are denoted as experimental cells. The cells with $CuCl_2$ are control cells. The baseline concentration of the experimental cell electrolyte solution was 0.03 M $PdCl_2$ and 0.3 M LiCl in D_2O, as used in previously reported co-deposition investigations (Refs. 2 to 6). For a control cell, the baseline electrolyte concentration was 0.03 M $CuCl_2$ and 0.3 M LiCl in D_2O. The LiCl is desired to support dissolution of the primary metallic salt. The salts were placed in a vial and capped. Plastic mesh lattice pieces were used to support the electrode wires. The clean platinum wire was passed through the plastic lattice as appears in Figure 2(a). The gold wires were placed on the lattice as shown in Figure 2(b). Blue CR-39 solid state nuclear track detector chips were also attached to this cathode lattice construction.

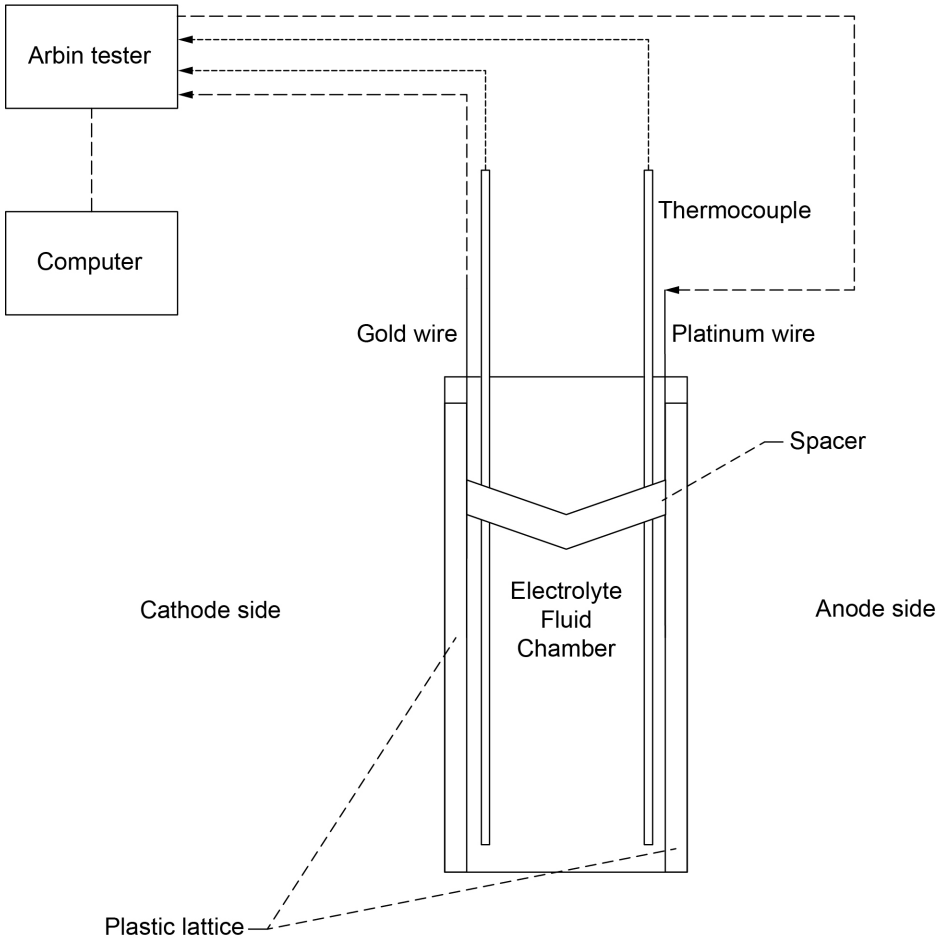

Figure 1.—Test system diagram for single electrolysis cell. Single bubble detector was placed outside cell behind electrolyte chamber as shown.

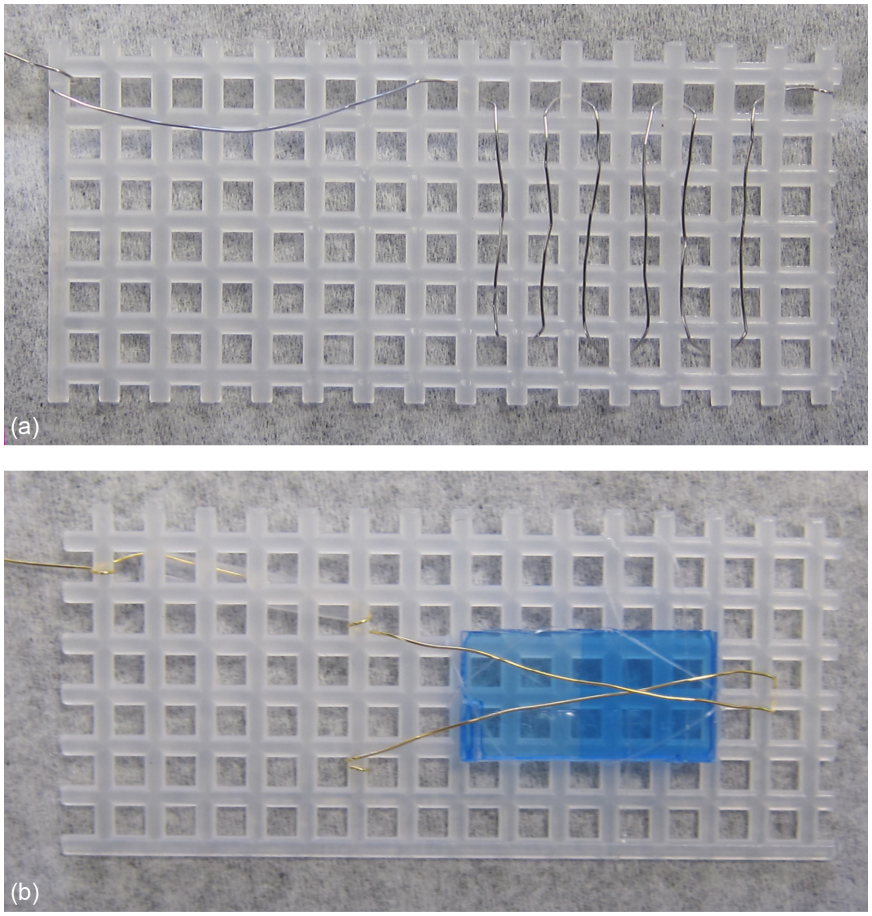

Figure 2.—Electrode wire configurations on lattice structure. (a) Platinum anode wire wrapped so there are six horizontal crossings on lattice. (b) Gold cathode wire arranged in “V” shape and secured to lattice over Columbia Resin 39 solid-state nuclear track detector.

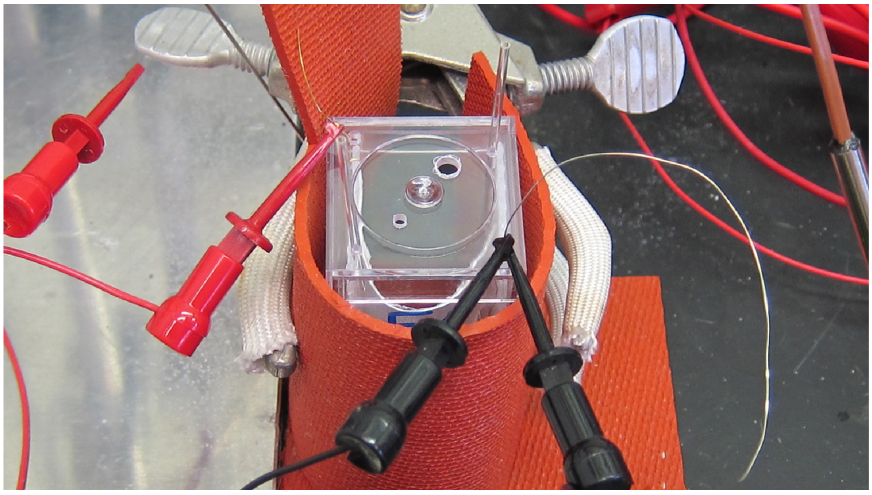

Figure 3.—Angled view down on partially assembled electrolysis cell, showing securing clamp and silicone rubber.

The two lattice pieces retaining the electrode wires were placed into the acrylic cell. These two lattices were pressed apart by the polyethylene spacer that was bent to fit in between the electrodes, resulting in a nominal cathode-to-anode spacing of 2 cm. The acrylic cell cover was placed on top of the cell, and the electrode wires were positioned through predrilled holes. Glass capillary tubes were inserted into the remaining two small holes in the cover for protection of and to prevent contamination from thermocouple probes. Figure 3 shows a cell at this stage of assembly. The desired electrolyte solution was transferred by pipet into the acrylic cell through a center hole, and the initial fluid level was marked on the side of the cell before the unit was transferred to a fume hood, placed in a clamp, and loosely surrounded with silicone insulation to allow better grip with the clamp. This volume of electrolyte submerged approximately 9 cm of gold wire and 18 cm of platinum wire. Once secured by the clamp, the appropriate electrical supply and monitoring leads were attached to the electrode wires.

Bubble Technology Industries Personal Neutron Dosimeters were used for neutron detection and placed behind the cells, midway between the electrodes with the cathode always to the left, as is shown in Figure 4. These dosimeters were calibrated for sensitivity within the range of 0.88 to 3.2 bubbles per microsievert. Detectors were capped and reset between periods of usage. A complete listing of detector serial numbers and calibrations in bubbles per millirem is provided in Appendix A. Although a sievert is the proper SI radiation dose unit, the scaling of millirem allows calibration presentation in whole-numbered bubble counts.

All were operated at room temperature inside of a fume hood. Figure 5 shows how cells were typically arranged within the fume hood. During early trials, only two cells were operated at a time, whereas later trials involved as many as eight cells operating simultaneously. Still, the cells were spaced at least 8 cm apart.

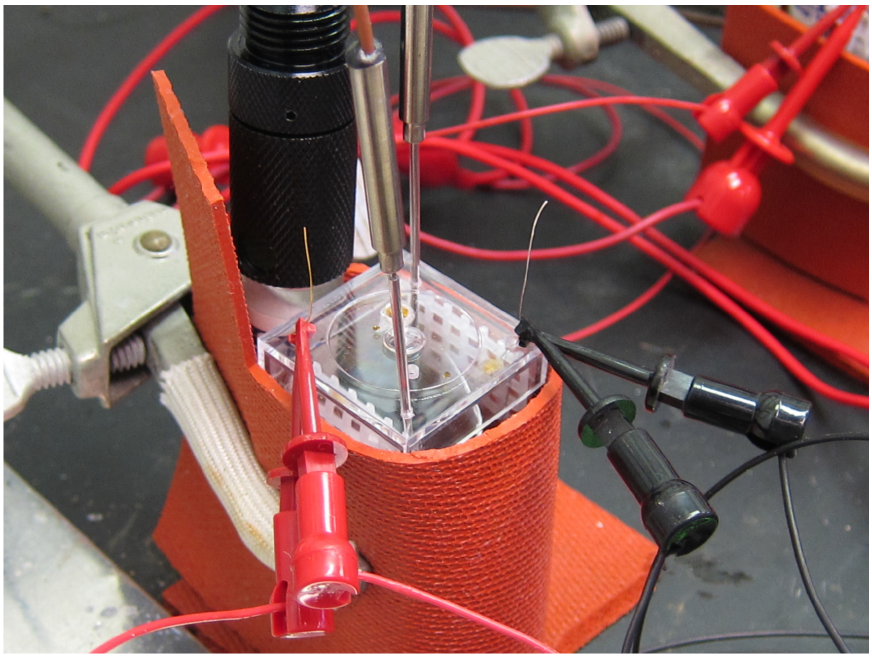

Figure 4.—Electrolysis cell as it appears when completely assembled with gold cathode (left) and platinum anode (right) wires visible. Bubble detector is securely placed behind cell.

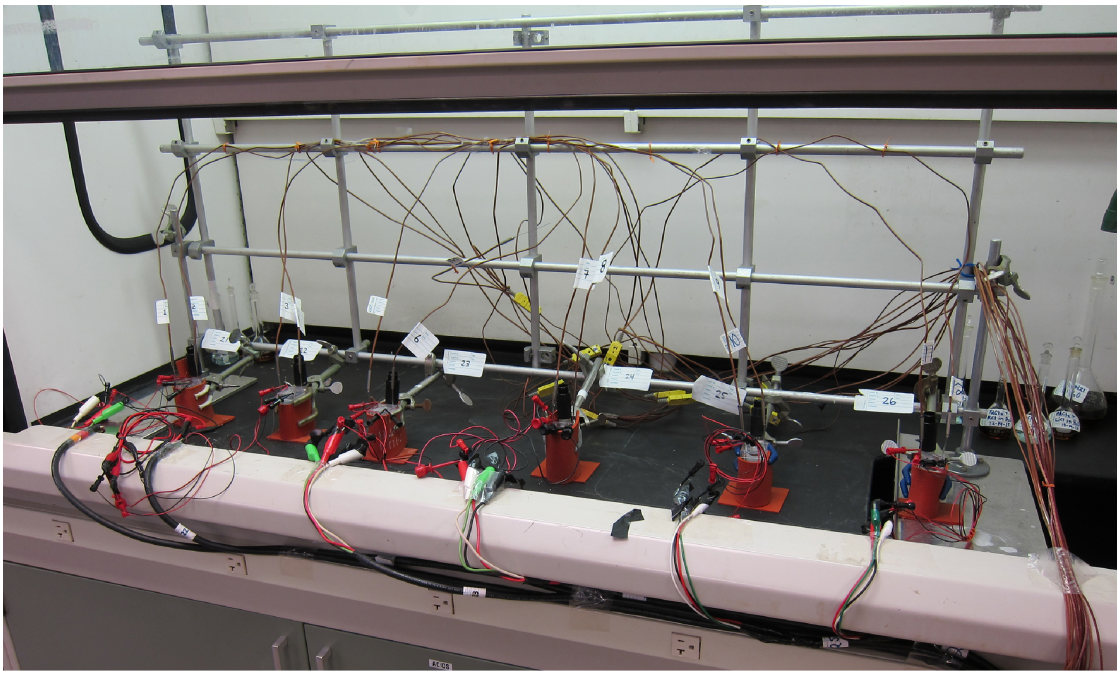

Figure 5.—Example electrolysis cells arrangement within fume hood.

Cell current was controlled using an Arbin BT-2000 battery tester programmed to supply either the standard current profile given in Table I or the comparatively rapid profile provided in Table II. These two profiles were derived from the profiles used in previous studies (Refs. 2 to 5, and 7). This instrument was chosen for the capability to provide desired currents up to 100 mA with ±0.1 percent accuracy and to monitor voltage with a sensitivity of ±100 mV. The current direction from anode to cathode promotes co-deposition of palladium and deuterium onto the gold cathode in experimental cells and co-deposition of copper and deuterium in control cells.

Cells were given names in the following form: Trial (T)-Roman numeral-Cell type (E for Experimental or C for Control) and Arabic numeral. For example, the third Experimental cell of Trial IV is denoted as T-IV-E3. If there existed only one cell of a particular type in a trial, the final number is omitted. All experimental and control cells contained the same previously described electrolyte solutions, with the exceptions of (1) T-IV-E2 and T-IV-C2 where DI water replaced D_2O and (2) T-IV-E3 and T-IV-C3 where KCl replaced LiCl with mass adjusted to maintain the same molar concentration in the D_2O solution. Refer to Table III for a complete listing of cell setup details. CR-39 track counts were only taken for Trials III and V. Trials VIII and X incorporated DU initially attached to the cathode lattice as presented in Figure 6. For cells T-IX-E1 and T-IX-C1, magnets were placed externally to the cells as shown in Figure 7.

Bubble detectors were visually counted once per day for bubbles appearing between the rounded dosimeter bottom and the start of a sticker label located midway across the unit. For reference, Figure 8 shows many bubbles dispersed throughout the bubble detector polymer media. Additional cell maintenance consisted of daily visual inspections of electrical connections and additions of pure D_2O, or DI water for T-IV-E2 and T-IV-C2, to maintain the initial fluid level to ensure the electrodes remained sufficiently submerged, since the cells were of an open, unpressurized design that allowed normal evaporation.

TABLE I.—STANDARD CURRENT-TIME PROFILE FOR CELL ELECTROLYSIS

Step	Duration, hr:min	Current, mA
1	0:05	0.0
2	24:00	0.1
3	24:00	0.2
4	284:00	0.5
5	24:00	5.0
6	24:00	10.0
7	24:00	25.0
8	24:00	50.0
9	≥24:00[a]	100.0
10	0:05	0.0

[a]The duration of Step 9 was often extended to postpone completion of a trial.

TABLE II.—RAPID CURRENT-TIME PROFILE FOR CELL ELECTROLYSIS

Step	Duration, hr:min	Current, mA
1	0:05	0.0
2	24:00	0.1
3	24:00	0.5
4	24:00	1.0
5	24:00	5.0
6	24:00	25.0
7	24:00	100.0
8	0:05	0.0

TABLE III.—SUMMARY OF TRIALS, CELLS, AND SETUP DETAILS

Trial	Cell	Current profile	Electrolyte	Additional[a]
I	E	Standard	$PdCl_2$, LiCl, D_2O	
I	C	↓	$CuCl_2$, LiCl, D_2O	
II	E	↓	$PdCl_2$, LiCl, D_2O	
II	C	↓	$CuCl_2$, LiCl, D_2O	
III	E1	↓	$PdCl_2$, LiCl, D_2O	
III	E2	↓	$PdCl_2$, LiCl, D_2O	
III	E3	↓	$PdCl_2$, LiCl, D_2O	
III	E4	↓	$PdCl_2$, LiCl, D_2O	
III	E5	↓	$PdCl_2$, LiCl, D_2O	
III	C	↓	$CuCl_2$, LiCl, D_2O	
IV	E1	↓	$PdCl_2$, LiCl, D_2O	
IV	E2	↓	$PdCl_2$, LiCl, H_2O	
IV	E3	↓	$PdCl_2$, KCl, D_2O	
IV	C1	↓	$CuCl_2$, LiCl, D_2O	
IV	C2	↓	$CuCl_2$, LiCl, H_2O	
IV	C3	↓	$CuCl_2$, KCl, D_2O	
V	E1	↓	$PdCl_2$, LiCl, D_2O	
V	E2	↓	$PdCl_2$, LiCl, D_2O	
V	E3	↓	$PdCl_2$, LiCl, D_2O	
V	C1	↓	$CuCl_2$, LiCl, D_2O	
V	C2	↓	$CuCl_2$, LiCl, D_2O	
V	C3	↓	$CuCl_2$, LiCl, D_2O	
VI	E	↓	$PdCl_2$, LiCl, D_2O	
VI	C	↓	$CuCl_2$, LiCl, D_2O	
VII	E	↓	$PdCl_2$, LiCl, D_2O	
VII	C	↓	$CuCl_2$, LiCl, D_2O	
VIII	E	↓	$PdCl_2$, LiCl, D_2O	Contains DU, 0.4132 g
VIII	C	▼	$CuCl_2$, LiCl, D_2O	Contains DU, 0.3374 g
IX	E1	Rapid	$PdCl_2$, LiCl, D_2O	Magnets surrounding cell
IX	E2	↓	$PdCl_2$, LiCl, D_2O	
IX	C1	↓	$CuCl_2$, LiCl, D_2O	Magnets surrounding cell
IX	C2	↓	$CuCl_2$, LiCl, D_2O	
X	E	↓	$PdCl_2$, LiCl, D_2O	Contains DU
X	C	↓	$CuCl_2$, LiCl, D_2O	Contains DU
XI	E	↓	$PdCl_2$, LiCl, D_2O	
XI	C	▼	$CuCl_2$, LiCl, D_2O	

[a]DU is depleted uranium.

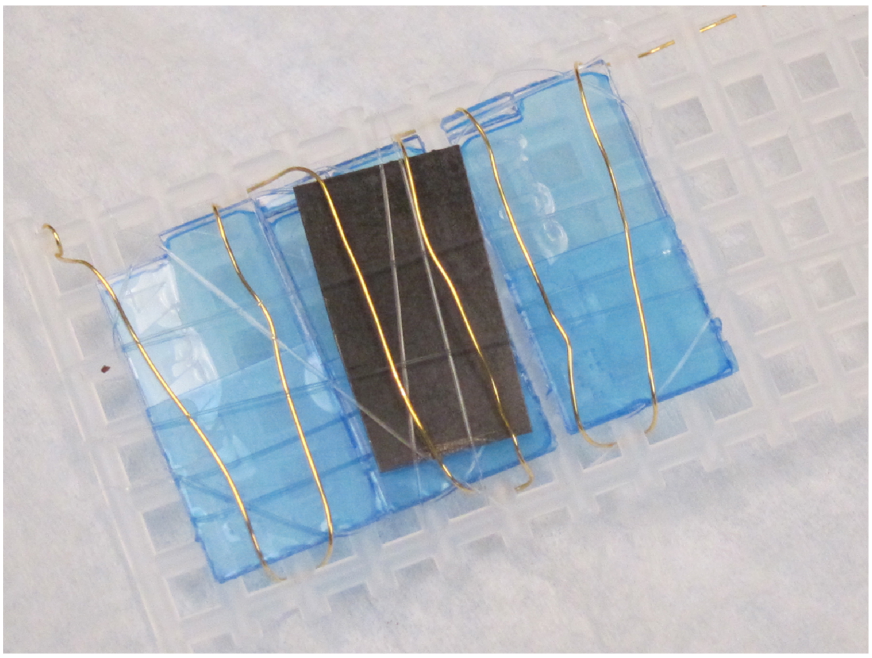

Figure 6.—Attachment of depleted uranium to cathode lattice of cell T-VIII-E prior to operation.

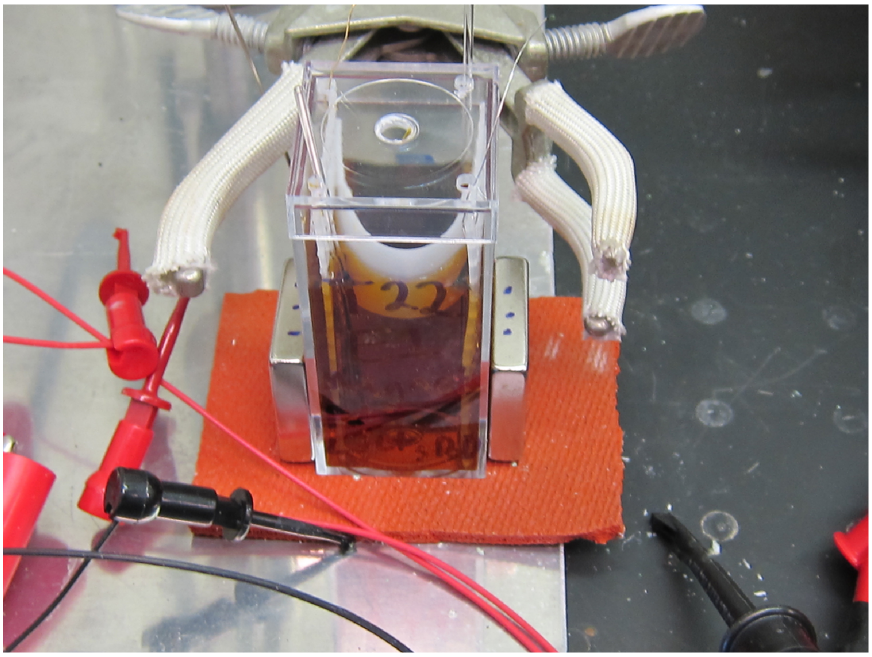

Figure 7.—Placement of magnets surrounding cell T-IX-E1. Magnets were located on cell exterior on sides with electrode lattices: cathode on left and anode on right.

Figure 8.—Bubble detector personal neutron dosimeters. Neutron-induced bubbles are visible in these three uncapped and used bubble detectors. Polymer detection media is translucent section to left of white label, which displays serial number and calibration data for each detector.

3.0 Data Analysis

The equivalent dose detected near each cell was defined as

$$H = \frac{b}{S} \tag{1}$$

where b is the total number of bubbles in the detector tube and S is the manufacturer-calibrated detector sensitivity in bubbles per microsievert. Daily averages and sample standard deviations were calculated for standard-configuration experimental cells as a set, and then for control cells as a separate set. Anderson-Darling (AD) tests were conducted to evaluate the data distribution normality and the appropriateness of further statistical treatments (Ref. 8). Calculated AD values were less than the AD critical value, indicating that there was insufficient evidence to reject the null hypothesis that the sample data were normally distributed. Therefore, subsequent analyses considered the data to be normally distributed.

Confidence intervals were calculated for the 95% confidence level using a Student's t-test. For days during a test without a bubble detector reading, total bubble counts were linearly interpolated between data recordings for the purposes of calculating averages and confidence intervals. Differences in the mean values between experimental and control cells were evaluated using a two-tailed Welch's unequal variance t-test, with the null hypothesis being that the means were equal. This test was selected because of the unequal sample sizes in the experiment and control populations.

4.0 Results

4.1 Cell Operation and Observations

Cell voltage, as a function of applied current, was used as a cell health and electrical continuity metric. It was generally the first indicator of a poor connection somewhere in the circuit. In total, 13 experimental cells and 9 control cells completed the entire current-time profile in the standard test configuration previously described. While electrolyte temperature was monitored for each cell, no temperature differences were observed between experimental and control cells using type K thermocouples that typically provide accuracy to ±2.2 °C.

Deposition material adherence is a function of electrolyte solute concentrations and the current-time profile (Ref. 7) In Figure 9, it is shown that the electrolyte solution was colorless and nearly clear following the standard electrolytic protocol. Both experimental and control cells, which were amber and blue, respectively, prior to applying current, appeared similarly clear following standard testing. This is evidence that most of the initial salt cations were removed from solution by the current-time protocol. With the shortened, rapid protocol, the electrolyte clarity was not achieved. In general, high initial concentrations and greater supplied current levels early in cell operation resulted in minimal cathode deposition and larger quantities of wasted material collecting on the cell bottom. Also in Figure 9, a comparison is provided for the physical results of more rapid current increases early in a current-time profile. Plating appears incomplete with a visible gradient in solution and minimal adherence to the cathode, more similar to the initial condition than the end state of cells that followed the standard profile.

The palladium cathodes tended to show dendritic macrostructures prior to deconstruction of the cells. Once removed from the cell interior, the electrodes generally appeared as presented in Figure 10. In the depleted uranium trials, the DU material mostly dissolved into solution, forming a dark sludgy mixture like that shown in Figure 11.

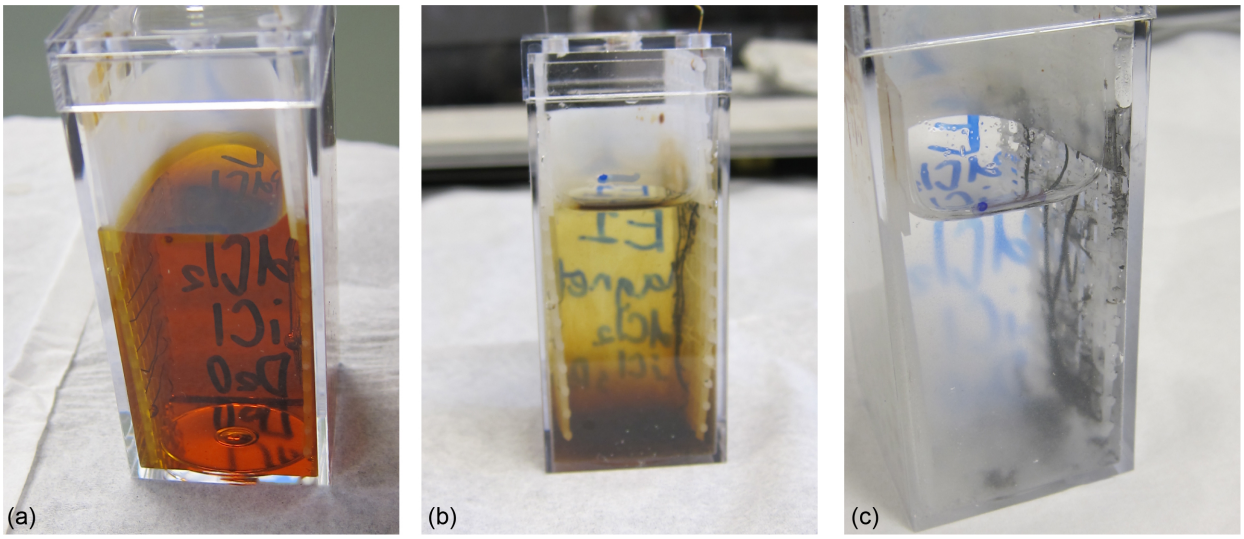

Figure 9.—Assembled experimental cell images. (a) Cell T-VI-E prior to operation. (b) Experimental cell following rapid current profile. (c) T-VI-E after test.

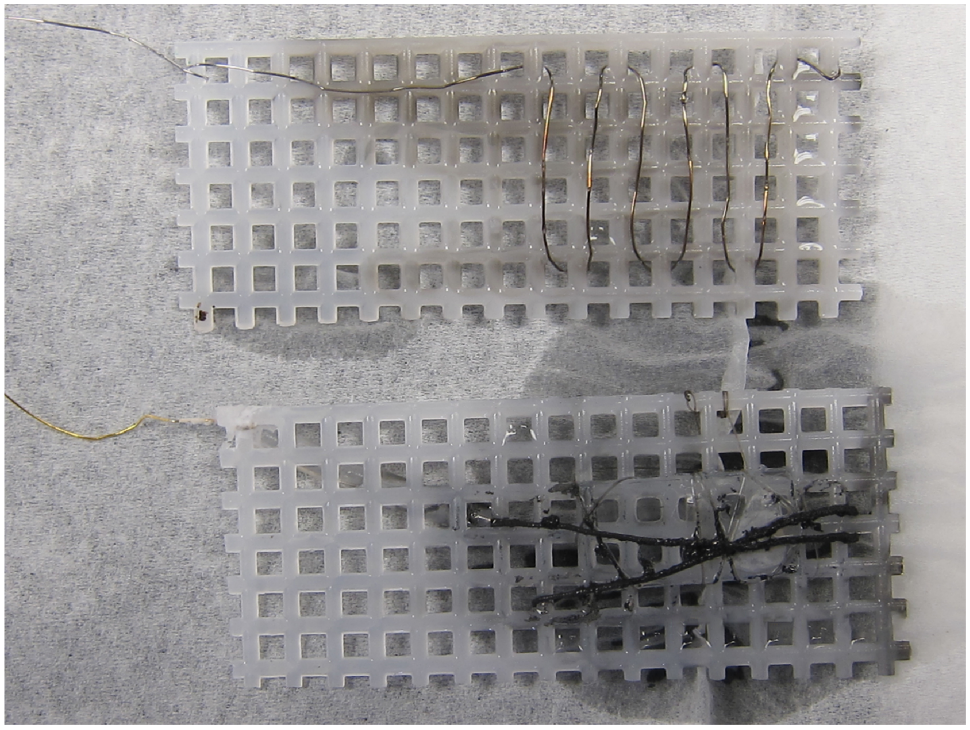

Figure 10.—T-III-E1 anode, top, and cathode, bottom, posttest.

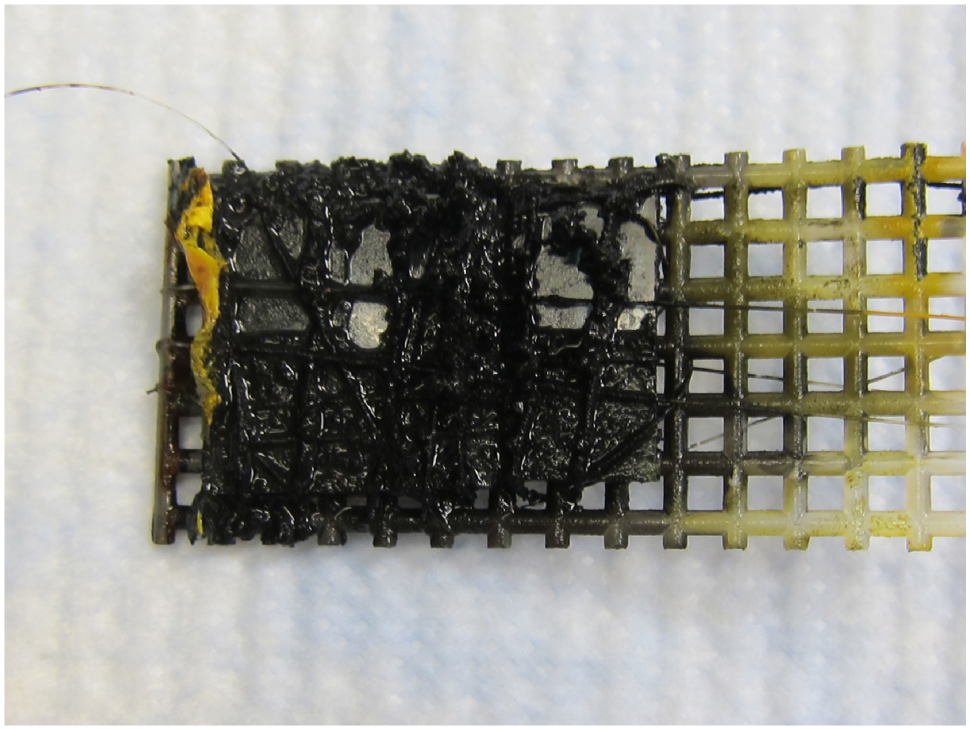

Figure 11.—Depleted uranium residue on cathode lattice of cell T-VIII-E posttesting and after cell disassembly.

4.2 Radiation Measurements

In Figure 12, the radiation doses detected for each standard configuration cell—excluding the special cases such as the KCl cells—and the standard applied current profile are presented over the test duration. Although there is overlap between experimental and control cell results, the general trend appears that experimental cells produce more radiation than the control cells. This inspired further statistical analysis of the raw data presented in Appendix B.

Average radiation levels detected for both cell groups are reported in Figure 13. Radiation levels detected near the experimental cells are, on average, greater than that measured near the control cells for the entirety of the test profile from test start to the end of the current-time profile. The upper and lower 95% confidence intervals are presented for the average cumulative radiation dose per cell, calculated for the experimental cells and the control cells as separate groups without pooling the variances. This visually presents the statistically significant separation in neutron emissions between the experimental and control cells. The lower 95% confidence interval limit of the experimental cell is greater than the upper 95% confidence interval limit of the control cell from test days 9 through 20. Additionally, for the same test day range, the Welch's t-test shows that there is significantly more average cumulative radiation detected near experimental cells compared with that from control cells at a 99% confidence level ($p < 0.01$).

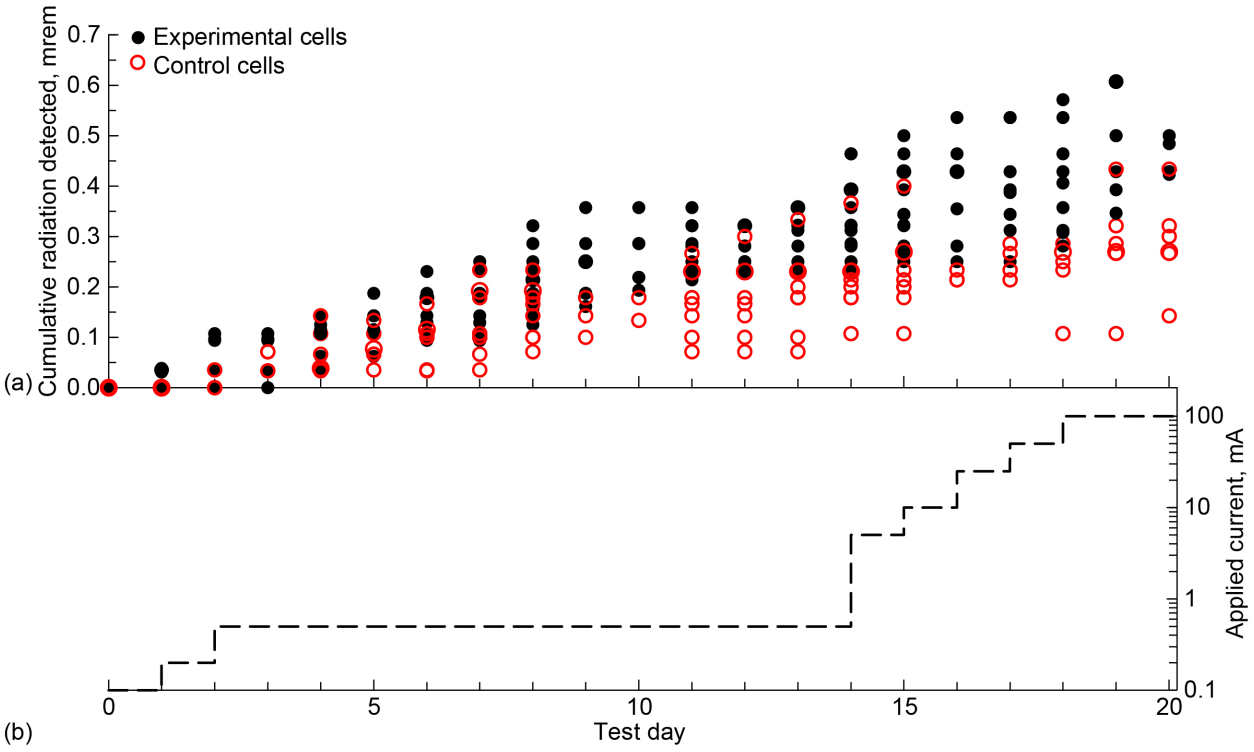

Figure 12.—Electrolysis cell results over test duration in days. (a) Cumulative radiation, or equivalent dose, detected for each cell. (b) Current supplied to cells during each run.

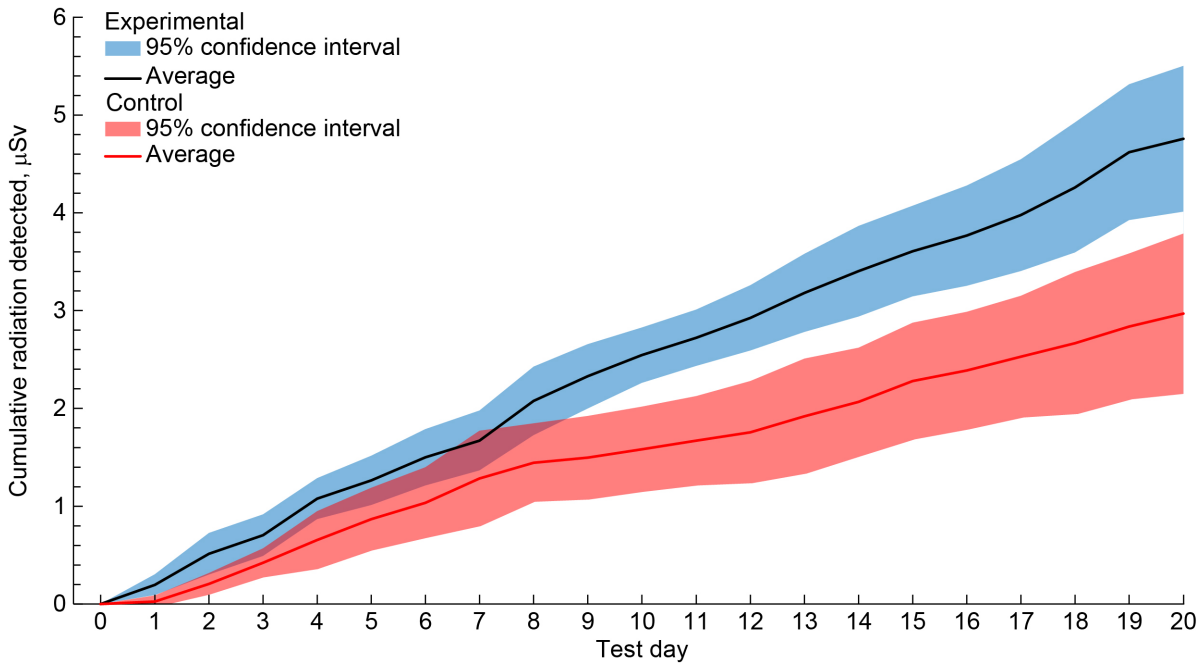

Figure 13.—Average radiation dose detected with 95% confidence intervals for experimental and control cells over test duration.

To compare to the standard configuration, two pairs of cells were constructed in a manner to either replace the D_2O (as in T-IV-E2 and T-IV-C2) or LiCl (as in T-IV-E3 and T-IV-C3). The bubble detector radiation detection measurements are provided in Figure 14 and Figure 15 for this trial. There is no clear distinction between these experimental and control cells from any of these measurements, as would be expected if D_2O and LiCl are necessary for any component of this process such as solute dissolution or a reaction process. A background measurement, from a bubble detector within the same fume hood but located more than 12 in. from any operating cells, is shown in both plots and was higher than either Pd-containing cell for much of the test duration. Based upon CR-39 analysis, previous co-deposition experiments suggest that neutron producing reactions may still be possible with either water substituted for D_2O or KCl in place of LiCl (Ref. 4). It is possible that bubble detectors located exterior to a cell are not sensitive enough to enable discernment of such reduced emissions over only a single trial.

Figure 16 shows the bubble detector results for the two trials that involved DU. With the standard current profile, the control cell bubble detector actually detected more radiation. Using the rapid current profile, the experimental cell produced slightly more detected radiation. Looking at only single trials, there is no definitive result from either run, but it is clear that the setup used, simply attaching DU near the cathode, did not profoundly improve cell performance in any way.

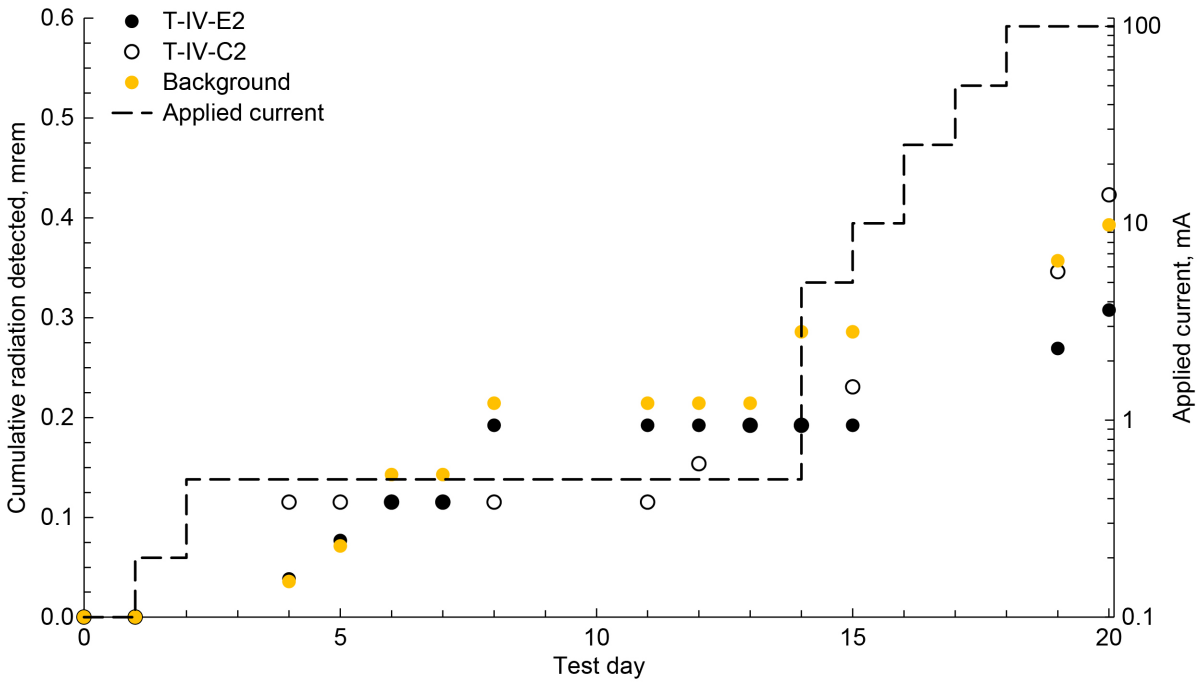

Figure 14.—Trial IV bubble detector results for cells replacing heavy water with de-ionized water, E2 and C2, compared to background measurement.

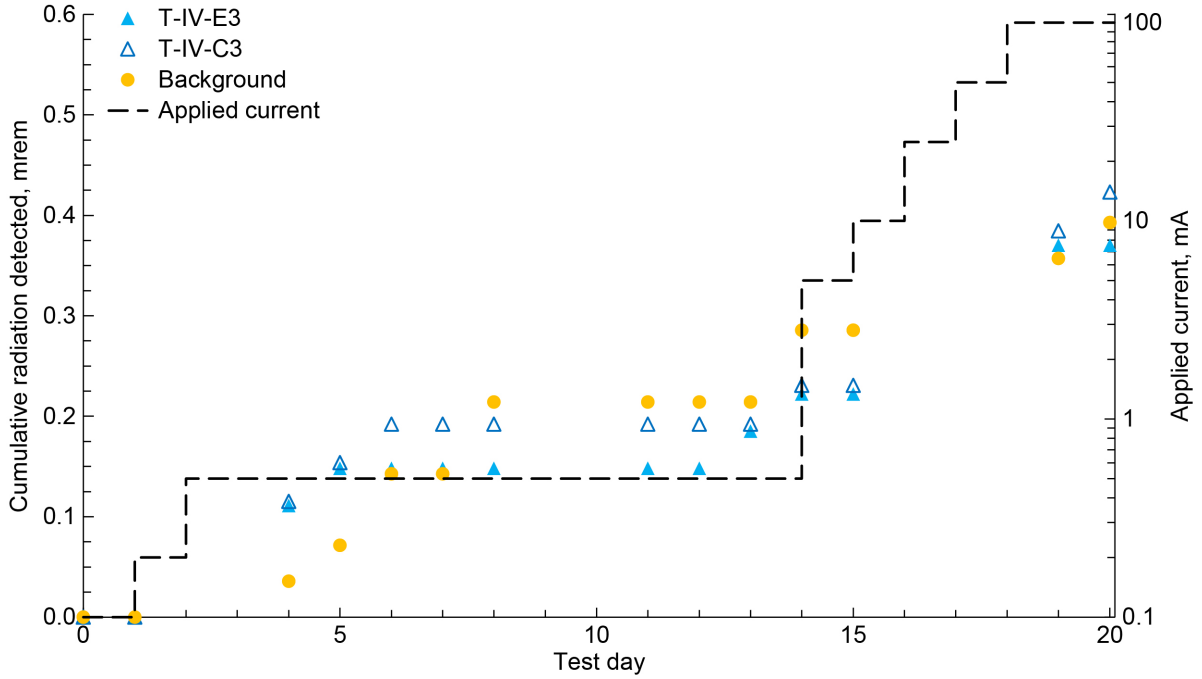

Figure 15.—Trial 19 bubble detector results for cells replacing LiCl with KCl, E3 and C3, compared to background measurement.

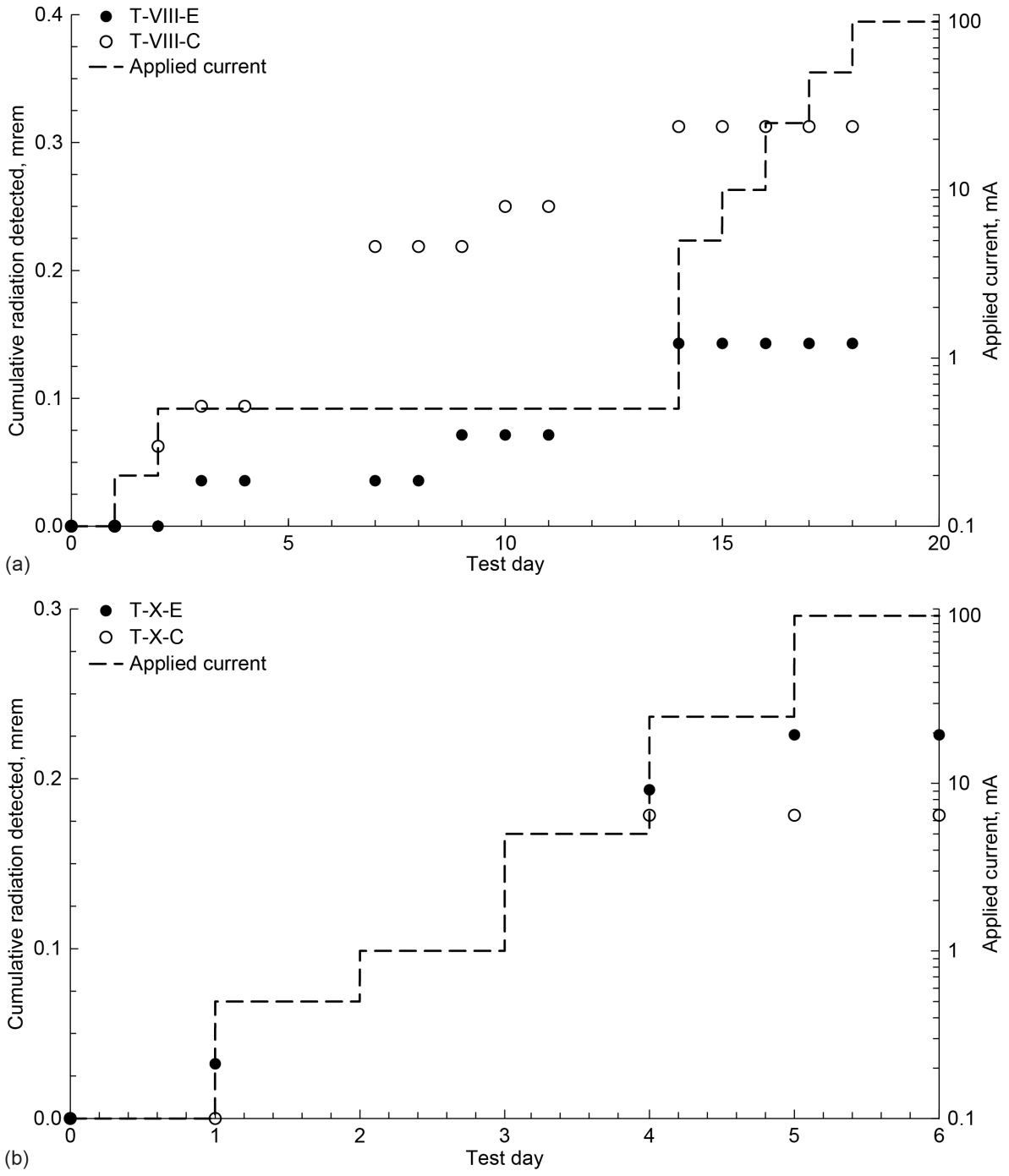

Figure 16.—Bubble detector results trials including depleted uranium. (a) Trial VIII. (b) Trial X.

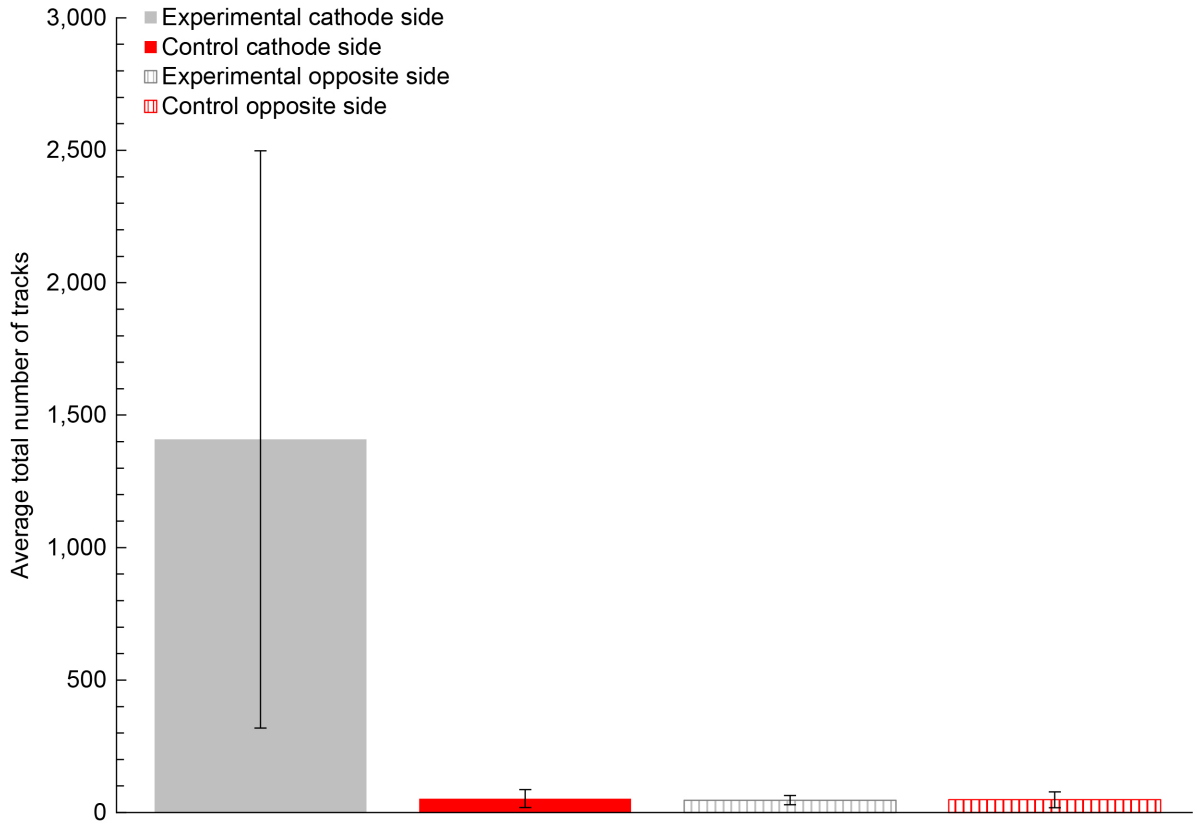

Figure 17.—CR-39 average track counts and 99.9% confidence intervals for Trials III and V.

Analyzing the results for the two standard trials with CR-39 detection, Figure 17 presents the average number of tracks counted on each side of chips from eight experimental cells and four control cells. For experimental cells, there were statistically significant track counts on the chip cathode side (i.e., facing the cathode wire). Six out of eight chips had track counts exceeding 1,000 on this surface. There was no significant difference between the opposite side of the experimental cell chips (i.e., facing away from the bulk of the cell) and either side of the control cell chips: all track counts were less than 75. Since all the chips were completely submerged in the electrolyte solutions, the electrolyte solution itself cannot account for this result.

5.0 Discussion

5.1 Measurement Uncertainty

The journal article previously discussing these tests (Ref. 1) included discussion on the uncertainties and potential for error related to the usage of bubble detectors. It is plausible that some of the neutrons recorded by the control cell bubble detectors may have originated from experimental cells. Four detectors each were uncapped to record fume hood radiation either while a trial was in process or when no testing was occurring. The average results of this are presented in Figure 18. When cells were operating within the fume hood, the average radiation dose detected was similar to the experimental average, even though the detectors were not adjacent to any particular cell. Without any operational cells present, background dosages were lower, more similar to the control average. This comparison is ultimately inconclusive

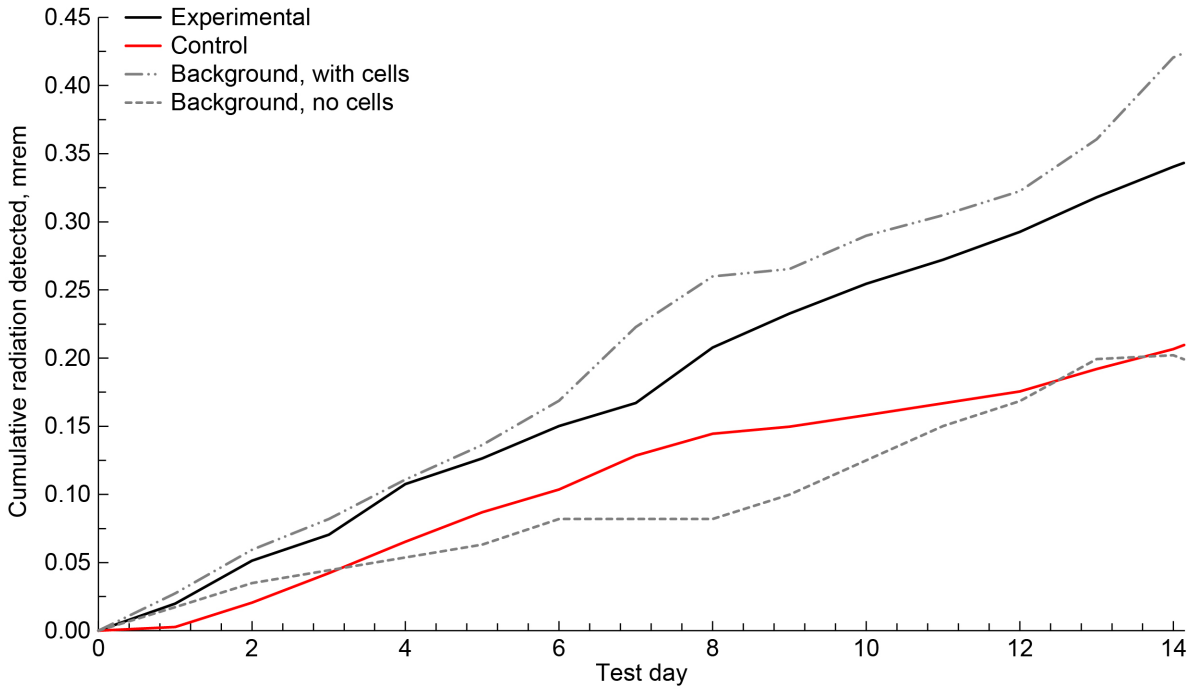

Figure 18.—Comparison of average radiation dosage measurements between experimental cells, control cells, and the background with and without cells running.

because of the small sample size, although it hints at the possibility that a true control average may be lower than what is presented here. Many control cells were operated with active experimental cells located to the left and the right of the control.

5.2 Dendritic Structure Significance

As discussed in the journal article, there appears to be some association between dendritic deposits on cathodes and observed neutron activity. Dendrites are clearly visible on the cathode surface of the T-III-E1 cell in Figure 19, which produced the greatest total neutron dose and dose per day of all observed cells. That cell is also notable for the relative electrolyte clarity and lack of deposits at the bottom of the cell at the end of the test run. For comparison, several post-test images are also presented in Figure 20 and Figure 21 to show the electrolyte condition and quantity of deposits on the cell bottom for other test runs. These images present an overhead view of each cell shortly following discontinuation of applied current and removal of the cell lid.

In Figure 20, two cells that produced below average neutron doses are presented next to T-III-E1. In the below-average cells, the majority of the palladium is at the bottom of the cell. Although a considerable amount of the palladium fell to the bottom of the cells, T-V-E1 and T-V-E2 cells still produced higher neutron doses than the corresponding control cells. In Figure 21, three average-performing experimental cells are displayed for assessment. More of the palladium is concentrated on or near the cathode surface, rather than as deposits allowed to clump and fall to the floor of the cell. Still, none of these cells presented the dendritic structure as evidently as T-III-E1.

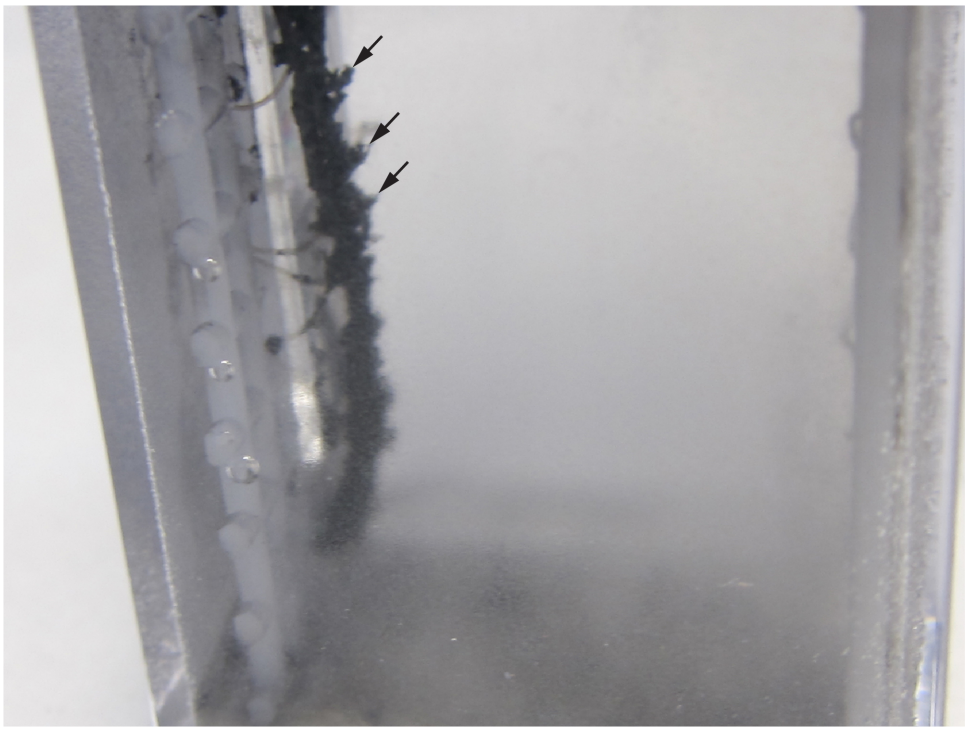

Figure 19.—Dendritic structure on the cathode surface of the best performing experimental cell (T-III-E1).

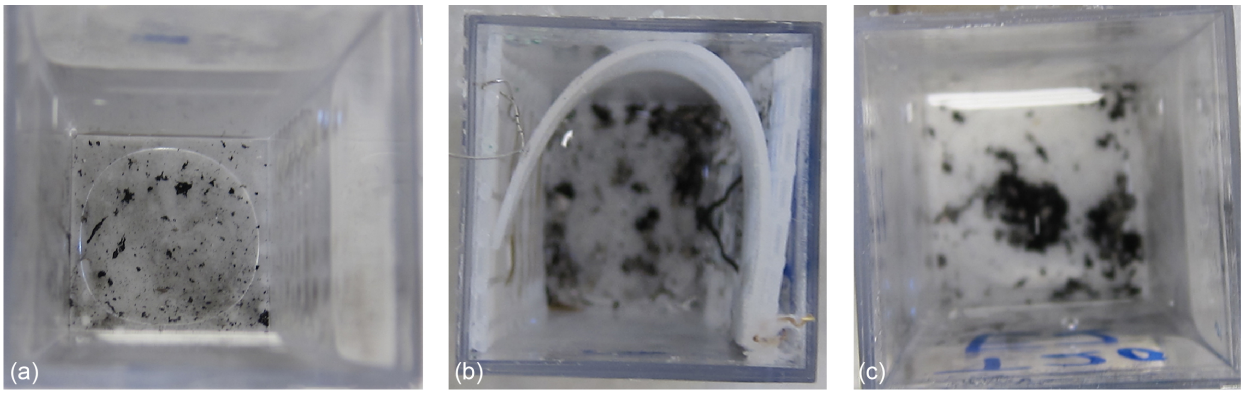

Figure 20.—Overhead posttest images of best performing experimental cell (T-III-E1) compared with two below-average-performing experimental cells upon removal of cell lid. (a) T-III-E1. (b) T-V-E1. (c) T-V-E2.

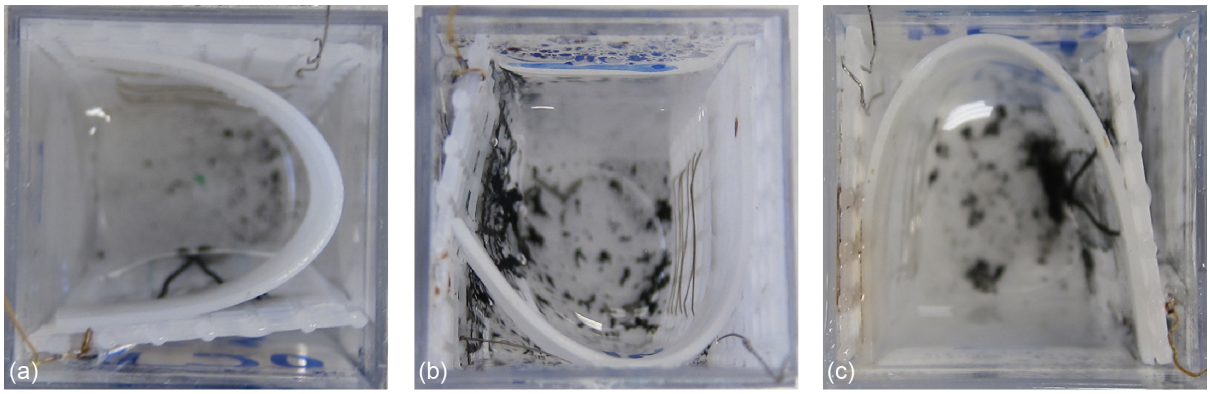

Figure 21.—Overhead posttest images of three average-performing experimental cells upon removal of cell lid. (a) Cell T-V-E3. (b) Cell T-IV-E1. (c) Cell T-VI-E.

5.3 Operational Reliability

No changes or improvements were made to cell construction throughout this work in an attempt to generate a sufficient collection of data from a single set of test conditions. This is one of the primary factors in limiting test duration to approximately 20 days. Whereas some cells operated successfully beyond that duration, many neared failure of the electrical circuit. Thinning and breakage of electrical test leads was common due to metals dissimilarity and contact with the corrosive electrolyte. The narrowness of the electrode wires contributed to fragility at many setup stages.

There are, however, many known potential upgrades to improve operational reliability. Test power and voltage monitoring connections are best attached with new, clean, and sturdy leads such as alligator clips, which will likely not displace even over several weeks or months. Thicker electrode wires reduce the likelihood of breakage over a given test duration from stress, corrosion, embrittlement, or electromigration. Wire drawing processes that preserve strength and elasticity also contribute to improved performance in this area.

6.0 Conclusions

A case control methodology was followed where a series of experimental and control electrochemical cells were constructed and then monitored with neutron dosimeters in the form of bubble detectors. Experimental cells were built using a previously published protocol, which showed previously evidence of neutron activity. In the standard configuration, these cells consisted of palladium(II) chloride, lithium chloride, and D_2O, with applied currents ranging from 0.1 to 100.0 mA over the test period of 20 days. Control cells were prepared with copper(II) chloride, lithium chloride, and D_2O ectrolyte as a means to document background cosmogenic neutron sources, using the same current profile. For this configuration, the bubble detector and CR-39 results provide evidence that there are significantly more neutrons generated by the experimental cells in comparison to the control cells. Single-trial alternative configurations consisted of using a shorter duration current-time profile, swapping KCl for LiCl, substituting water for D_2O, adding magnets to the cell exterior, or adding depleted uranium to the cell interior.

For an improved statistical comparison in future iterations, there should be equal quantities of experimental and control cells, not simply one control per test trial. An ideal setup requires sufficient spacing between operating cells to prevent measurement of emissions from an adjacent cell. Potential error could also be reduced through the additional use of an automated bubble detector counting machine,

placement of multiple detectors near each cell, and not switching detectors for bubble recompression during a trial. It would also be preferable to have CR-39 chips within every cell as a backup monitoring method, although resources were not available at the time of this testing to include them in the setup and analyze the chips after testing for every trial.

Most cells were not supplied current in excess of the 3-week duration because of reliability issues including corrosion of electrical test leads connecting to electrode wires, embrittlement of gold cathode wires exposed in electrolyte over time, and general brittleness of thin platinum wires causing interruptions of the circuit. There is also potential for lack of adhesion between deposits and the minimal available cathode wire surface area so that, over time, hydrogen evolution at the cathode disrupts the deposited material, which then collects at the bottom of the cell. This displaced material is less likely to continue contribution to neutron generation.

Appendix A.—Bubble Detector Calibrations

TABLE A.1.—BUBBLE DETECTOR SERIAL NUMBERS AND CALIBRATIONS USED FOR RADIATION MEASUREMENT

Serial number	Calibration, bubbles per millirem	Corresponding trials and cells
12265103	28	T-III-E1, T-III-E2, T-III-E3, T-III-E4, T-IV-E1
12265131	26	T-III-E2, T-III-E4, T-III-C, T-IV-E2, T-V-E1, T-IX-E1
12265138	30	T-III-E3, T-III-E4, T-III-C, T-IV-C1, T-V-C1, T-VI-C, T-IX-C2
12265139	28	T-I-E, T-III-E1, T-III-E4, T-V-E2, T-IX-E1, T-XI-E
12265149	28	T-II-E, T-III-E1, T-III-E2, T-III-E5, T-VIII-E, T-IX-E2
12265156	32	T-III-E2, T-III-E3, T-V-E3, T-VII-E1
12265158	28	T-I-C, T-III-E2, T-III-E3, T-III-E4, T-V-C3, T-X-C
12265217	28	T-II-C, T-III-E3, T-III-E5, T-IX-C1
12317214	32	T-III-E5, T-III-C, T-VIII-C
12317418	30	T-IX-E2, T-XI-C
12317428	31	T-VI-E, T-X-E
13144346	26	T-III-E5, T-III-C, T-IV-C3, T-V-C2, T-VI-C, T-IX-C1
13144427	26	T-III-E4, T-III-E5, T-III-C, T-IV-C2
13144429	27	T-III-E5, T-III-C, T-IV-E3
13144447	30	T-VII-C1, T-IX-C2

Appendix B.—Raw Data Tables

TABLE B.1.—BUBBLE DETECTOR TOTAL BUBBLE COUNTS BY DAY

(a) Trial numbers I, II, and III

Test day	Bubble count									
	T-I-E	T-I-C	T-II-E	T-II-C	T-III-E1	T-III-E2	T-III-E3	T-III-E4	T-III-E5	T-III-C
0	0	0	0	0	0	1	0	1	1	0
1			1	0	0	1	0	3	3	1
2			1	0	1	1	0	3	3	2
3	1	2			4	1	2	3	4	4
4	3	3								
5	3	3								
6	3	3	5	3	5	3	3	7	6	5
7	5	3	5	3	9	4	5	8	6	5
8			6	4	10	7	6	8	6	5
9			7	4	10	8	7	8	7	5
10					10	9	7	8	7	5
11	7	4								
12	7	4	9	5						
13	9	5	10	5	13	13	8	11	9	6
14	9	5	11	5	13	14	8	12	9	6
15			12	5	13	15	8	12	9	6
16			12	6	15	15	8	12	10	6
17	11	8			16	15	9	13	10	7
18	12	8								
19	14	9	17	8						
20	14	9	17	8	21	17	11	17	10	11
21	14	9								
22										
23					24	18	14	18	10	13
24	17	11			24	19	15	18	10	13
25										
26										
27					26	20	15	20	13	14
28										
29										
30					29	24	15	21	14	14
31					31	24	17	21	14	14
32										
33										
34					31	24	19	22	17	14
35										

TABLE B.1.—(Continued)

(a) Trial numbers I, II, and III

Test day	Bubble count									
	T-I-E	T-I-C	T-II-E	T-II-C	T-III-E1	T-III-E2	T-III-E3	T-III-E4	T-III-E5	T-III-C
36					32	25	21	23	19	14
37					33	26	21	25	19	15
38					33	27	22	25	19	15
39										
40										
41					39	29	27	27	21	16
42					39	29	27	28	21	16
43					39	30	27	28	22	17
44					39	30	27	28	22	17
45					41	30	28			18
46										
47										
48										
49					45	30	30			22
50					47	31	30			23
51					47	31	31			23
52					49	32	31			25
53										
54										
55					50	39	33			28

TABLE B.1.—(Continued)

(b) Trial numbers IV and V

Test day	Bubble count											
	T-IV-E1	T-IV-C1	T-IV-E2	T-IV-C2	T-IV-C3	T-IV-E3	T-V-E1	T-V-C1	T-V-E2	T-V-C2	T-V-E3	T-V-C3
0	0	0	0	0	0	0	0	0	0	0	0	0
1	1	0	0	0	0	0	1	0	0	0	0	0
2												
3												
4	3	1	1	3	3	3	3	2	4	1	2	1
5	4	4	2	3	4	4	3	2	4	2	2	1
6	5	5	3	3	5	4	6	3	4	3	3	1
7	5	7	3	3	5	4	6	3	4	5	3	1
8	6	7	5	3	5	4	6	5	5	5	4	2
9												
10												
11	9	8	5	3	5	4	6	5	6	6	9	2
12	9	9	5	4	5	4	6	5	7	6	9	2
13	9	10	5	5	5	5	6	6	7	6	10	2
14	10	11	5	5	6	6	6	6	8	6	10	3
15	11	12	5	6	6	6	7	6	9	7	11	3
16												
17												
18							8	7	10	7	13	3
19	12	13	7	9	10	10	9	8	11	7	16	3
20	12	13	8	11	11	10	11	8	12	7	16	4
21	13	14	8	12	11	12	11	8	12	7	16	4
22	14	16	11	12	11	13	11	9	13	7	16	4
23												
24												
25		17	11	14	13	16	12	9	16	11	18	8
26		17	12	15	15	16	12	10	16	11	18	10

TABLE B.1.—(Concluded)

(c) Trial numbers VI, VII, VIII, IX, X, and XI

Test day	Bubble count													
	T-VI-E	T-VI-C	T-VII-E1	T-VII-C1	T-VIII-E	T-VIII-C	T-IX-E1	T-IX-C1	T-IX-E2	T-IX-C2	T-X-E	T-X-C	T-XI-E	T-XI-C
0	0	0	0	0	0	0	0	0	0	0	0	0	0	0
1	1	0	0	0	0	0	0	1	0	0	1	0	0	0
2	3	0			0	2	1	1	0	0			2	2
3	3	1			1	3								
4					1	3					6	5		
5			6	2			3	5	2	2	7	5	5	
6	4	1	6	3			4	5	2	4	7	5	6	
7	4	2	6	3	1	7							6	
8	5	3	8	3	1	7							6	
9	5	3			2	7								
10	6	4			2	8								
11			9	3	2	8								
12			9	3										
13	10	7	9	3										
14	10	7			4	10								
15	10	7	11	6	4	10								
16	11	7			4	10								
17	12	8	11	7	4	10								
18					4	10								
19														
20	15	9												
21					8	12								
22					8	12								

References

1. Smith, Phillip J.; Hendricks, Robert C.; and Steinetz, Bruce M.: Electrolytic Co-Deposition Neutron Production Measured by Bubble Detectors. J. Electroanal. Chem., vol. 882, no. 115024, 2021. https://www.sciencedirect.com/science/article/pii/S1572665721000503 Accessed May 4, 2021.
2. Mosier-Boss, Pamela A., et al.: Triple Tracks in CR–39 as the Result of Pd-D Co-Deposition: Evidence of Energetic Neutrons. Naturwissenchaften, vol. 96, 2009, pp. 135–142. https://link.springer.com/article/10.1007/s00114-008-0449-x Accessed May 4, 2021.
3. Boss, Pamela A., et al.: System and Method for Generating Particles. U.S. Patent 8,419,919, 2013. https://patentimages.storage.googleapis.com/64/5c/30/7213209cf2a684/US8419919.pdf Accessed May 4, 2021.
4. Mosier-Boss, P.A., et al.: Use of CR–39 in Pd/D Co-Deposition Experiments. Eur. Phys. J. Appl. Phys., vol. 40, 2007, pp. 293–303.
5. Mosier-Boss, Pamela A.; Forsley, Lawrence P.; and McDaniel, Patrick J.: Investigation of Nano-Nuclear Reactions in Condensed Matter. Defense Threat Reduction Agency Final Report, 2016. https://www.lenr-canr.org/acrobat/MosierBossinvestigat.pdf Accessed May 4, 2021.
6. Szpak, S.; Mosier-Boss, P.A.; and Smith, J.J.: Deuterium Uptake During Pd-D Co-Deposition. J. Electroanal. Chem., vol. 379, 1994, pp. 121–127. https://www.sciencedirect.com/science/article/pii/0022072894871302 Accessed May 4, 2021.
7. Mosier-Boss, P.A., et al.: Detection of High Energy Particles Using CR–39 Detectors Part 1: Results of Microscopic Examination, Scanning, and LET Analysis. Int. J. Hydrog. Energy, vol. 42, no. 1, 2017, pp. 416–428. https://www.sciencedirect.com/science/article/pii/S0360319916330968 Accessed May 10, 2021.
8. Anderson, T.W.; and Darling, D.A.: A Test of Goodness of Fit. J. Am. Stat. Assoc., vol. 49, no. 268, 1954, pp. 765–769. https://www.tandfonline.com/doi/abs/10.1080/01621459.1954.10501232 Accessed May 10, 2021.